Science

RESEARCH ARTICLES

Cite as: Y. Liu *et al.*, *Science* 10.1126/science.abo2756 (2022).

An olivine cumulate outcrop on the floor of Jezero crater, Mars

Y. Liu[1]*, M. M. Tice[2], M. E. Schmidt[3], A. H. Treiman[4], T. V. Kizovski[3], J. A. Hurowitz[5], A. C. Allwood[1], J. Henneke[6], D. A. K. Pedersen[6], S. J. VanBommel[7], M. W. M. Jones[8], A. L. Knight[7], B. J. Orenstein[9], B. C. Clark[10], W. T. Elam[11], C. M. Heirwegh[1], T. Barber[1], L. W. Beegle[1], K. Benzerara[12], S. Bernard[12], O. Beyssac[12], T. Bosak[13], A. J. Brown[14], E. L. Cardarelli[1], D. C. Catling[15], J. R. Christian[7], E. A. Cloutis[16], B. A. Cohen[17], S. Davidoff[1], A. G. Fairén[18,19], K. A. Farley[20], D. T. Flannery[9], A. Galvin[1], J. P. Grotzinger[20], S. Gupta[21], J. Hall[13], C. D. K. Herd[22], K. Hickman-Lewis[23, 24], R. P. Hodyss[1], B. H. N. Horgan[25], J. R. Johnson[26], J. L. Jørgensen[6], L. C. Kah[27], J. N. Maki[1], L. Mandon[28], N. Mangold[29], F. M. McCubbin[30], S. M. McLennan[5], K. Moore[20], M. Nachon[2], P. Nemere[9], L. D. Nothdurft[9], J. I. Núñez[26], L. O'Neil[11], C. M. Quantin-Nataf[31], V. Sautter[12], D. L Shuster[32], K. L. Siebach[33], J. I. Simon[30], K. P. Sinclair[11], K. M. Stack[1], A. Steele[34], J. D. Tarnas[1], N. J. Tosca[35], K. Uckert[1], A. Udry[36], L. A. Wade[1], B. P. Weiss[13], R. C. Wiens[37], K. H. Williford[1,38], M.-P. Zorzano[18]

[1]Jet Propulsion Laboratory, California Institute of Technology, Pasadena, CA 91109, USA. [2]Department of Geology and Geophysics, Texas A&M University, College Station, TX 77843, USA. [3]Department of Earth Sciences, Brock University, St. Catharines, ON L2S 3A1, Canada. [4]Lunar and Planetary Institute, Universities Space Research Association, Houston TX 77058, USA. [5]Department of Geosciences, Stony Brook University, Stony Brook, NY 11794, USA. [6]Department of Space, Measurement and Instrumentation, Technical University of Denmark,, Lyngby, Denmark. [7]McDonnell Center for the Space Sciences, Department of Earth and Planetary Sciences, Washington University in St. Louis, St. Louis, MO 63130, USA. [8]Central Analytical Research Facility, and School of Chemistry and Physics, Queensland University of Technology, Brisbane, QLD 4000, Australia. [9]School of Earth and Atmospheric Sciences, Queensland University of Technology, Brisbane, QLD 4000, Australia. [10]Space Science Institute, Boulder, CO 80301, USA. [11]Applied Physics Lab and Department of Earth and Space Sciences, University of Washington, Seattle, WA 98052, USA. [12] Institut de Minéralogie, Physique des Matériaux et Cosmochimie, Centre National de la Recherche Scientifique (CNRS), Muséum National d'Histoire Naturelle, Sorbonne Université, Paris 75005, France. [13]Department of Earth, Atmospheric and Planetary Sciences, Massachusetts Institute of Technology, Cambridge, MA 02139, USA. [14]Plancius Research, MD 21146, USA. [15]Department of Earth and Space Sciences, University of Washington, Seattle WA 98195, USA. [16]Department of Geography, University of Winnipeg, Winnipeg, Manitoba R3B 2E9, Canada. [17]NASA Goddard Space Flight Center, Greenbelt, MD 20771, USA. [18]Centro de Astrobiología, Consejo Superior de Investigaciones Cientificas - Instituto Nacional de Tecnica Aeroespacial, Madrid 28850, Spain. [19]Dept. of Astronomy, Cornell University, Ithaca, NY 14853, USA. [20]Division of Geological and Planetary Sciences, California Institute of Technology, Pasadena, CA 91125, USA. [21]Department of Earth Science and Engineering, Imperial College London, London SW7 2AZ, UK. [22]Department of Earth and Atmospheric Sciences, University of Alberta, Edmonton, Alberta T6G 2E3, Canada. [23]Department of Earth Sciences, The Natural History Museum, South Kensington, London, SW7 5BD, UK. [24]Dipartimento di Scienze Biologiche, Geologiche e Ambientali, Università di Bologna, via Zamboni 67, I-40126 Bologna, Italy. [25]Department of Earth, Atmospheric, and Planetary Sciences, Purdue University, West Lafayette, IN 47907, USA. [26]Johns Hopkins University Applied Physics Laboratory Laurel, MD 20723, USA. [27]Department of Earth and Planetary Sciences, University of Tennessee, Knoxville TN 37996, USA. [28]Laboratoire d'Etudes Spatiales et d'Instrumentation en Astrophysique, Observatoire de Paris-Université Paris Sciences et Lettres, CNRS, Sorbonne Université, Université de Paris Cité, Meudon 92190, France. [29]Laboratoire Planetologie et Geosciences, Centre National de Recherches Scientifiques, Universite Nantes, Universite Angers, Unite Mixte de Recherche 6112, Nantes 44322, France. [30]NASA Johnson Space Center, Houston, TX 77058, USA. [31]Laboratoire de Geologie de Lyon-Terre Planetes Environnement, Univ Lyon, Universite Claude Bernard Lyon 1, Ecole Normale Superieure Lyon, Centre National de Recherches Scientifiques, 69622 Villeurbanne, France. [32]Dept. Earth and Planetary Science, University of California, Berkeley, CA 94720, USA. [33]Department of Earth, Environmental, and Planetary Sciences, Rice University, Houston, TX 77005, USA. [34]Earth and Planets Laboratory, Carnegie Institution for Science, Washington, DC 20015, USA. [35]Department of Earth Sciences, University of Cambridge, Cambridge, CB2 3EQ, UK. [36]Department of Geosciences University of Nevada Las Vegas, Las Vegas, NV 89154, USA. [37]Los Alamos National Laboratory, Los Alamos, NM 87545, USA. [38]Blue Marble Space Institute of Science, 600 1st Ave. Seattle, WA 98104, USA.

***Corresponding author. Email: yang.liu@jpl.nasa.gov**

The geological units on the floor of Jezero crater, Mars, are part of a wider regional stratigraphy of olivine-rich rocks, which extends well beyond the crater. We investigate the petrology of olivine and carbonate-bearing rocks of the Séítah formation in the floor of Jezero. Using multispectral images and x-ray fluorescence data, acquired by the Perseverance rover, we performed a petrographic analysis of the Bastide and Brac outcrops within this unit. We find that these outcrops are composed of igneous rock, moderately altered by aqueous fluid. The igneous rocks are mainly made of coarse-grained olivine, similar to some Martian meteorites. We interpret them as an olivine cumulate, formed by settling and enrichment of olivine through multi-stage cooling of a thick magma body.

Jezero crater, the landing site of the Perseverance rover, is located at the western edge of Isidis Planitia on Mars (Fig. 1A). Orbital data has constrained the crater's age to between 3.82 and 3.96 Ga (*1*, *2*). A light-toned, olivine- and carbonate-

bearing rock unit exposed on the floor of Jezero has been informally named the Séítah formation (Fig. 1C) (*3*–*5*). Rocks similar to Séítah in morphology and mineralogy extend beyond the rim of Jezero; they span >70,000 km^2 from inside Isidis Planitia (*6*), to the neighboring regions of Northeast Syrtis (*7*), Nili Fossae (*8*), and Libya Montes (Fig. 1B) (*9*, *10*). Orbital observations have shown this regional unit has high abundances of olivine (*11*), an early crystallizing, rock-formimg mineral, with large inferred grain sizes (several millimeters) and moderate magnesium contents of Fo_{44-66}. (where Fo is forsterite, Mg_2SiO_4, and the subscript numbers indicate its molar percentage in olivine) (*4*, *11*). Hypotheses for the unit's origin include an impact melt or intrusive igneous rocks (*6*), basaltic lava flows (*9*, *12*), volcanic ash (*2*, *13*) or clastic material (fragmental deposits formed by transport and deposition from volcanic eruptions, impacts, water, or wind) (*14*).

Images of Séítah formation rocks taken by the Perseverance rover have shown centimeter- to decimeter-scale layering and abundant dark, millimeter-scale angular grains, reported in a companion paper (*5*). These observations were consistent with any of the above hypotheses for the regional unit's origin. We sought to distinguish between these possibilities using the rover's arm-mounted Planetary Instrument for X-ray Lithochemistry (PIXL) (*15*).

PIXL observations

To remove any modified surface materials, two 50 mm diameter patches (informally named Garde and Dourbes) were abraded into two rock outcrops (informally named Bastide and Brac, respectively). Both outcrops are part of the Bastide member (informal name) of the Séítah formation (Fig. 1C). Reflectance optical images of both patches, illuminated by ultraviolet (UV, 385 nm), blue (B, 450 nm), green (G, 530 nm) and near-infrared (735 nm) light emitting diodes (LEDs) were acquired using PIXL's micro context camera (MCC). The Dourbes patch was subsequently analyzed to produce two x-ray fluorescence (XRF) raster maps with areas of 4 × 12.5 mm and 5 × 7 mm, at a step size of 0.125 mm (Fig. 1) (*16*).

We use these data to produce color and color ratio images of both patches, and estimate volume percentages of phases in each (Fig. 2A, fig. S1, and table S1). For the Dourbes patch where XRF maps were acquired, we produce diffraction maps of crystallinity and crystal orientation (Fig. 2C and fig. S2), composite maps of elemental abundances (Fig. 2D and figs. S3 and S4), and chemical analyses of individual minerals and the bulk rock (tables S2 and S3) (*16*). The reconstructed color images show both patches display a similar texture, with beige equant grains of sizes range from 1 to 3.5 mm, greenish gray irregularly shaped grains, and reddish brown materials rimming these grains or occupying irregular areas between them (fig. S1A). These features are discernable in color ratio plots (Fig. 2A and fig. S1). Elemental maps show inter-grain areas that contain distinct chemical variations, and additional irregular regions with high Al (Fig. 2D) and non-uniform distribution of Na, K, and P (fig. S3).

Our identifications of olivine and pyroxene minerals are supported by stoichiometric analysis of the PIXL data and are consistent with observations by other Perseverance instruments (*5*). We find the beige equant grains have molar (Mg+Fe)/Si ≈ 2 and total cations of 2.995 - 3.025 per 4 oxygens (table S2), consistent with olivine's chemical formula $(FeMg)_2SiO_4$. The greenish gray grains have molar (Ca+Mg+Fe)/Si ≈ 1 and total cations of 4.032 – 4.042 per 4 oxygens (table S2), consistent with pyroxene's formula $(CaFeMg)_2Si_2O_6$. The molar Ca/(Ca+Mg+Fe) ratios of the pyroxene (0.35 to 0.37) show that it is the mineral augite (Fig. 3A) (*17*). Back-reflected diffracted x-rays from some non-contiguous augite regions show that they have identical crystal orientations, indicating these regions are likely to be part of the same three-dimensional grain (i.e., a single augite crystal) (Fig. 2C and fig. S2). This texture, where a large single pyroxene grain encloses smaller olivine grains (poikilitic texture), is characteristic of igneous cumulate rocks (Fig. 2, A and B). The irregular inter-grain Al-rich areas contain intergrown grains of Na-rich feldspar (<1 mm), Fe-Cr-Ti oxide (≤0.25 mm), K-rich feldspar (<0.125 mm) and Ca-phosphate (<0.125 mm), which are typical features of mesostasis – the last formed materials in the intergranular space – in igneous rocks (figs. S3 and S4). Olivine, augite, and mesostasis are the primary minerals in the pre-alteration bedrocks in the Séítah formation. The inter-grain reddish brown materials contain silicates, Fe-Mg carbonate, and Fe-Mg sulfate, which are secondary materials from alteration. The presence of carbonates was also indicated by other instruments on Perseverance (*5*) and consistent with oribital observations. We focus our analysis on the primary minerals.

Olivine is the dominant primary mineral, making up 65 ± 5 vol% of the Dourbes and Garde rocks (fig. S1B and table S1). The remainder of the analyzed area is made of augite at ~13 vol%, mesostasis at ~10 vol%, and secondary materials at ~12 vol %. The relative mineral proportions of olivine, augite, and feldspar (Fig. 3C) indicate Dourbes is an olivine-rich wehrlite, a type of ultramafic igneous rock (*18*).

The chemical compositions of the olivine grains ($Fo_{55 \pm 1}$) are uniform, both within and between grains (Fig. 3B and table S2). Olivine grains contain more Fe than that would be in equilibrium with a melt of the rocks' bulk composition (fig. S5 and tables S2 and S5). The augite composition is $Wo_{35-38}En_{43-44}Fs_{20-21}$, expressed as molar percentages of wollastonite (Wo, $Ca_2Si_2O_6$), enstatite (En, $Mg_2Si_2O_6$), and ferrosilite (Fs, $Fe_2Si_2O_6$) (Fig. 3A). Some regions in the single large poikilitic augite grain we investigated have small variations in Ca (<0.7 wt% Ca), Fe (<0.6 wt%), Mg (<0.6 wt) and Cl (~0.3 wt%) (table

S3). These could indicate the presence of inclusions, thin lamellae of pyroxene of different compositions, and/or minor alteration products that are smaller than PIXL's x-ray beam size.

Fe/Mn ratios of olivine and pyroxene in meteorites have been used to determine their planetary parentage (*19*). The molar Fe/Mn ratios in Martian meteorites are 47 ± 3 for olivine and 32 ± 6 for pyroxene (uncertainties are 1 standard deviation) (*19*). The Dourbes minerals have ranges of molar Fe/Mn ratios of 55 ± 8 to 67 ± 9 for olivine and 38 ± 13 to 42 ± 3 for augite. The lower ends of these ranges are consistent with the values found for meteorites; we speculate that the higher Fe/Mn values could be due to a small amount of Fe-bearing minerals formed from aqueous alteration of olivine.

Mesostasis areas show few signs of secondary salts; they have low abundances of SO_3 and Cl and all analyzed element abundances sum to ~94.0 – 99.5 wt% (table S4), indicating the presence of little-to-no additional material enriched in C or H, which PIXL cannot detect directly. Compositions of the Fe-Cr-Ti oxide grains in Dourbes vary, depending on their petrographic setting. Those embedded in olivine have high molar Cr/Ti (~10), those at olivine-pyroxene boundaries have moderate Cr/Ti (~3.6), and those in mesostasis have low Cr/Ti (1-1.9) (fig. S6), leading to the variations in their estimated chemistry (table S4). Calcium phosphate occurs only in the mesostasis and has molar Ca/P ratios most consistent with merrillite (9:7) (fig. S7).

Interpretation as an igneous cumulate

We use our observations to evaluate the hypotheses mentioned above for the origin of olivine-carbonate unit exposed in Seitah.

Volcaniclastic (e.g., pyroclastic deposits) or impact clastic (e.g., rock fragments cemented by quenched impact melt) origins typically produce heterogeneous mixtures of mineral grains and rock fragments, embedded in a fine-grained matrix of (or altered from) ash particles (<50 μm). For Brac and Bastide outcrops in the Séítah formation, there is no evidence of rock fragments or a zoned fine-grained texture (Fig. 1). Observations of other outcrops also reveal no evidence of heterogeneous mixtures (*5*). We therefore exclude this possibility.

Sedimentary deposition of detrital olivine grains with cements is unlikely. The observed assemblage of coarse-grain augite and mesostasis with feldspar and Fe-Cr-Ti oxides has not previously been observed as a sedimentary cement, and would not precipitate from fluids at near-surface temperatures and pressures. These grains are also too coarsely crystalline to be a detrital matrix. It is also not likely that the entire abrasion patch sits within one rock fragment in an extremely coarse-grained water-transported clastic rock (i.e., a conglomerate), because there is no evidence in images of the host rock for pebble-sized or larger grain boundaries, cements or fine-grained matrix, hydraulic sorting, sedimentary structures, erosion, or channel forms, as would be expected for such a deposit (*5*).

Instead, we conclude that the olivine and augite formed by cooling of a magma body. The magma could have arisen from volcanism or an impact, because impact melting can fully homogenize the target rock, which would then solidify and crystalize very similarly to a volcanic magma originating from the Martian mantle. We interpret Brac to be a cumulate igneous rock formed by settling and accumulation of olivine crystals from a molten mafic magma. The observed poikilitic texture is common in cumulate rocks on Earth (*20*) and in several Martian meteorites (*21*). The compositional trend in Cr/Ti ratios we observed in the Fe-Cr-Ti oxide grains is also consistent with oxides crystallizing from a cooling magma (fig. S6). The similarity in mineralogy (*5*), textures, color, and reflectance spectral properties between Brac and Bastide within the Séítah formation indicates that our cumulate lithology interpretation can be extrapolated beyond the Dourbes abraded patch.

Petrogenetic history

We next consider the magmatic crystallization and cooling history of the olivine cumulate outcrops in the Séítah formation. Using the chemistry of the olivine (fig. S5), we infer that the magma was more iron rich, with Mg# = 27 to 30 (where Mg# is the molar Mg/(Mg+Fe) × 100) (*16*), than previously found (Mg# = 52 to 67) for Martian meteorites (*22*, *23*). We suggest that Séítah cumulate rocks formed from a parent magma that had previously lost Mg-rich minerals. Brac is different in both mineralogy and bulk chemistry from olivine-rich cumulates in Martian meteorites, and also from olivine-rich rocks at Gusev crater investigated by the Spirit rover (Figs. 3 and 4A) (*16*). The olivine grain size distribution and uniform composition in Brac, as well as the lack of larger olivine crystals observed in any Séítah outcrops, indicates an initially crystal-free melt (Fig. 5B). The presence of similar sized olivine grains indicates an early stage of rapid homogeneous olivine nucleation, due to oversaturation, possibly induced by rapid cooling (Fig. 5C). Additionally, the presence of melt inclusions (typically 100-300 μm, with one up to ~600 μm) in the Dourbes olivine grains (Fig. 2D and fig. S4) suggests early rapid growth of olivine, forming crystals with open space between their outside faces (hopper or skeletal shaped crystals), typical morphology under rapid cooling (*24*). Later, olivine crystal of euhedral shapes formed through additional olivine growth filling in the open space, before or during gravitational settling (Fig. 5C). The gravitational settling forms a framework of olivine grains of mostly point contact with open space between grains (Fig. 5D). There is little textural or chemical evidence for later olivine growth filling in the open space, indicating that the cumulate was

unaffected by subsequent magma infiltration or exchange after the olivine crystals had formed and accumulated. The proportion (~35 vol%) of other minerals among the olivine is consistent with the expected porosity of an olivine cumulate unaffected by compaction (*25*). The chemical equilibrium of olivine and augite and the coarse grains of augite implies extended cooling at a temperature (~1085°C) below that olivine starts to crystallize (*16*).

Emplacement history

Olivine cumulates can form in different geological settings, including large layered mafic intrusions (LLMIs), thick lava flows/ponds, shallow intrusive bodies as sills/laccoliths, or thick melt sheets from large impacts or their melt ejecta (Fig. 5A). The emplacement environment of cumulate rocks as observed in the Séítah formation can be assessed using Earth analogs, after considering the difference in gravity (*16*). Unlike similar rocks in Earth LLMIs (*20*), Séítah olivine grains host large melt inclusions and show negligible additional growth after the olivine framework formed, indicating that Brac formed at depths of no more than a few kilometers. Thick (100-150 m) mafic or ultramafic lava flows or ponds on Earth form uncompacted frameworks of euhedral to subhedral olivine, similar to those observed in the Séítah formation. However, among Earth examples, olivine grains are typically smaller and the mesostasis is more fine-grained (or glassy) than in Séítah rocks (*16*). This indicates that these Martian cumulates experienced later cooling at a lower rate than Earth analogs. We suggest potential explanations of a thicker lava than on Earth; or emplacement into hot surroundings (e.g., a crystal laden lava injecting into a still-hot flow); or an intrusive environment such as a sill or a laccolith (a lens-shaped igneous formation). Alternatively, similar features could have formed in a super-heated impact melt sheet.

In those environments, olivine cumulates represent only the lower portion of the petrogenetic sequence. On Earth, pyroxene-rich cumulates commonly occur stratigraphically above olivine-rich layers, with a trend of minerals increasing in Fe, Na, and K higher in the sequence (Fig. 5D). Similar petrogenetic sequences have been hypothesized for cumulate Martian meteorites (*26–28*). The overlying Máaz formation could consist of such rocks (*5*); however, the contact between the Séítah and Máaz formations is obscured along the rover traverse, preventing a definitive determination of their relationship (*5*). Alternatively, the originally overlying strata might not have been explored by the rover; could have been eroded; or there is no petrographic link between the Séítah and Máaz formations.

Regional and Planetary Context

The presence of olivine cumulates in Jezero crater constrains the origin of the more widespread olivine-bearing regional units in Isidis Planitia. On petrologic evidence alone, it is most plausible that emplacement of the Séítah olivine cumulate was by magma injection into an environment that permitted slow cooling, such as a shallow igneous intrusion in the Martian crust or into existing lava flows (*6*). However, this interpretation does not necessarily extend to the regional scale. A single large shallow intrusion seems unlikely to explain a regional unit over such a wide area (>70,000 km^2) with diverse local topographical influences. Similarly, the cumulate rock does not support the hypothesis that the regional unit is formed by a single deposit of clastic material (volcanic ash, impact ash or sediments). We suggest that the regional exposure represents a series of related intrusive (sills, laccoliths) and extrusive magma bodies (lava flows, pyroclastic deposits). It could also contain some reworked sedimentary derivatives of the igneous rocks.

Abundances of incompatible elements, (those that preferentially partition in the melt, e.g., Na, K, Rb, Sr, La, Sm, Nd, Yb, U, Th), in igneous rocks constrain the mantle source compositions. Ratios of rare earth elements (e.g, La/Yb) are often used. However, these elements are of low abundances (typically at parts per million or parts per billion by weight) that are below PIXL's detection limit. The abundance ratio of K_2O/TiO_2 can be used instead to constrain source characteristics, provided the magma has not experienced crystallization and removal of K- or Ti-bearing minerals (*29*). We compare our results to meteorites and igneous rocks studied by other rovers. The weight K_2O/TiO_2 ratio (0.38 ± 0.48) of the unaltered portion of Dourbes falls in the range found in Martian meteorites containing olivine cumulates (chassignite) or augite cumulates (nakhlite), as well as mafic rocks investigated by other Mars rovers and landers (Fig. 4B). All these samples are enriched in highly incompatible elements (e.g., K, U, and Th) compared to Ti (*30*). Measurements of Sm-Nd and Rb-Sr isotopes in nakhlites and chassignites have indicated that their mantle sources were depleted in highly incompatible elements; this suggests enrichment of highly incompatible elements in these cumulate meteorites during melt separation from the mantle sources (*26*, *28*). A process that enriches highly incompatible elements – possibly driven by interaction with high-temperature aqueous fluids after rock formation (metasomatic processes) – has previously been suggested for the mantle source regions of meteorites (*31*), alkali-rich basalts in Gusev crater (*32*) and Gale crater (*33*, *34*). Alternatively, geophysical data and models have been interpreted as indicating that Mars' mantle is depleted overall in radioactive heat producing (K, U, Th) and other highly incompatible elements, implying that those elements are instead concentrated in the planet's crust or upper mantle (*35*). Elevated abundances of highly incompatible elements in the mantle source regions at Gusev, Gale, and Jezero craters, as well as those for chassignites and nakhlites (*31*),

could indicate a general enrichment of such elements in Mars' upper mantle, possibly caused by metasomatic processes and/or plume activity. These different samples range from a formation age of > 3.9 Ga to 1.34 Ga (*3*, *36*). This wide range of ages and geographic locations of igneous rocks with these properties indicate a long-lived process that has been operating on Mars for billions of years and has affected a large fraction of Mars's crust and upper mantle (*16*).

REFERENCES AND NOTES

1. S. C. Werner, The early martian evolution—Constraints from basin formation ages. *Icarus* **195**, 45–60 (2008). doi:10.1016/j.icarus.2007.12.008
2. L. Mandon, C. Quantin-Nataf, P. Thollot, N. Mangold, L. Lozac'h, G. Dromart, P. Beck, E. Dehouck, S. Breton, C. Millot, M. Volat, Refining the age, emplacement and alteration scenarios of the olivine-rich unit in the Nili Fossae region, Mars. *Icarus* **336**, 113436 (2020). doi:10.1016/j.icarus.2019.113436
3. B. L. Ehlmann, J. F. Mustard, S. L. Murchie, F. Poulet, J. L. Bishop, A. J. Brown, W. M. Calvin, R. N. Clark, D. J. D. Marais, R. E. Milliken, L. H. Roach, T. L. Roush, G. A. Swayze, J. J. Wray, Orbital identification of carbonate-bearing rocks on Mars. *Science* **322**, 1828–1832 (2008). doi:10.1126/science.1164759 Medline
4. A. J. Brown, C. E. Viviano, T. A. Goudge, Olivine-carbonate mineralogy of the Jezero Crater region. *J. Geophys. Res. Planets* **125**, JE006011 (2020). doi:10.1029/2019JE006011 Medline
5. K. A. Farley *et al.*, Aqueously altered igneous rocks on the floor of Jezero crater, Mars. *Science* 10.1126/science.abo2196 (2022).
6. T. M. Hoefen, R. N. Clark, J. L. Bandfield, M. D. Smith, J. C. Pearl, P. R. Christensen, Discovery of olivine in the Nili Fssae region of Mars. *Science* **302**, 627–630 (2003). doi:10.1126/science.1089647 Medline
7. M. S. Bramble, J. F. Mustard, M. R. Salvatore, The geological history of Northeast Syrtis Major, Mars. *Icarus* **293**, 66–93 (2017). doi:10.1016/j.icarus.2017.03.030
8. B. L. Ehlmann, J. F. Mustard, An in-situ record of major environmental transitions on early Mars at Northeast Syrtis Major. *Geophys. Res. Lett.* **39**, 1–7 (2012). doi:10.1029/2012GL051594
9. L. L. Tornabene, J. E. Moersch, H. Y. McSween Jr., V. E. Hamilton, J. L. Piatek, P. R. Christensen, Surface and crater-exposed lithologic units of the Isidis Basin as mapped by coanalysis of THEMIS and TES derived data products. *J. Geophys. Res.* **113** (E10), E10001 (2008). doi:10.1029/2007JE002988
10. J. L. Bishop, D. Tirsch, L. L. Tornabene, R. Jaumann, A. S. McEwen, P. C. McGuire, A. Ody, F. Poulet, R. N. Clark, M. Parente, N. K. McKeown, J. F. Mustard, S. L. Murchie, J. Voigt, Z. Aydin, M. Bamberg, A. Petau, G. Michael, F. P. Seelos, C. D. Hash, G. A. Swayze, G. Neukum, Mineralogy and morphology of geologic units at Libya Montes, Mars: Ancient aqueously derived outcrops, mafic flows, fluvial features, and impacts. *J. Geophys. Res. Planets* **118**, 487–513 (2013). doi:10.1029/2012JE004151
11. A. Ody, F. Poulet, J.-P. Bibring, D. Loizeau, J. Carter, B. Gondet, Y. Langevin, Global investigation of olivine on Mars: Insights into crust and mantle compositions. *J. Geophys. Res. Planets* **118**, 234–262 (2013). doi:10.1029/2012JE004149
12. V. E. Hamilton, P. R. Christensen, Evidence for extensive, olivine-rich bedrock on Mars. *Geology* **33**, 433–436 (2005). doi:10.1130/G21258.1
13. C. H. Kremer, J. F. Mustard, M. S. Bramble, A widespread olivine-rich ash deposit on Mars. *Geology* **47**, 677–681 (2019). doi:10.1130/G45563.1
14. A. D. Rogers, N. H. Warner, M. P. Golombek, J. W. Head 3rd, J. C. Cowart, Areally extensive surface bedrock exposures on Mars: Many are clastic rocks, not lavas. *Geophys. Res. Lett.* **45**, 1767–1777 (2018). doi:10.1002/2018GL077030 Medline
15. A. C. Allwood, L. A. Wade, M. C. Foote, W. T. Elam, J. A. Hurowitz, S. Battel, D. E. Dawson, R. W. Denise, E. M. Ek, M. S. Gilbert, M. E. King, C. C. Liebe, T. Parker, D. A. K. Pedersen, D. P. Randall, R. F. Sharrow, M. E. Sondheim, G. Allen, K. Arnett, M. H. Au, C. Basset, M. Benn, J. C. Bousman, D. Braun, R. J. Calvet, B. Clark, L. Cinquini, S. Conaby, H. A. Conley, S. Davidoff, J. Delaney, T. Denver, E. Diaz, G. B. Doran, J. Ervin, M. Evans, D. O. Flannery, N. Gao, J. Gross, J. Grotzinger, B. Hannah, J. T. Harris, C. M. Harris, Y. He, C. M. Heirwegh, C. Hernandez, E. Hertzberg, R. P. Hodyss, J. R. Holden, C. Hummel, M. A. Jadusingh, J. L. Jørgensen, J. H. Kawamura, A. Kitiyakara, K. Kozaczek, J. L. Lambert, P. R. Lawson, Y. Liu, T. S. Luchik, K. M. Macneal, S. N. Madsen, S. M. McLennan, P. McNally, P. L. Meras, R. E. Muller, J. Napoli, B. J. Naylor, P. Nemere, I. Ponomarev, R. M. Perez, N. Pootrakul, R. A. Romero, R. Rosas, J. Sachs, R. T. Schaefer, M. E. Schein, T. P. Setterfield, V. Singh, E. Song, M. M. Soria, P. C. Stek, N. R. Tallarida, D. R. Thompson, M. M. Tice, L. Timmermann, V. Torossian, A. Treiman, S. Tsai, K. Uckert, J. Villalvazo, M. Wang, D. W. Wilson, S. C. Worel, P. Zamani, M. Zappe, F. Zhong, R. Zimmerman, PIXL: Planetary instrument for x-ray lithochemistry. *Space Sci. Rev.* **216**, 134 (2020). doi:10.1007/s11214-020-00767-7
16. Materials and methods are available as supplementary materials.
17. N. Morimoto *et al.*, Nomenclature of pyroxenes. *Am. Mineral.* **73**, 1123–1133 (1988).
18. R. W. Le Maitre *et al.*, *Igneous rocks: a classification and glossary of terms* (Cambridge University Press, Cambridge, United Kingdom, Second., 2002).
19. J. J. Papike, J. M. Karner, J. M. Shearer, Determination of planetary basalt parentage: A simple technique using the electron microprobe. *Am. Mineral.* **88**, 469–472 (2003). doi:10.2138/am-2003-2-323
20. L. R. Wager, The major element variation of the layered series of the Skaergaard intrusion and a re-estimation of the average composition of the hidden layered series and of the successive residual magmas. *J. Petrol.* **1**, 364–398 (1960). doi:10.1093/petrology/1.3.364
21. R. R. Rahib, A. Udry, G. H. Howarth, J. Gross, M. Paquet, L. M. Combs, D. L. Laczniak, J. M. D. Day, Mantle source to near-surface emplacement of enriched and intermediate poikilitic shergottites in Mars. *Geochim. Cosmochim. Acta* **266**, 463–496 (2019). doi:10.1016/j.gca.2019.07.034
22. D. S. Musselwhite, H. A. Dalton, W. S. Kiefer, A. H. Treiman, Experimental petrology of the basaltic shergottite Yamato-980459: Implications for the thermal structure of the martian mantle. *Meteorit. Planet. Sci. Arch.* **41**, 1271–1290 (2005).
23. J. B. Balta, H. Y. McSween, Water and the composition of martian magmas. *Geology* **41**, 1115–1118 (2013). doi:10.1130/G34714.1
24. F. Faure, P. Schiano, G. Trolliard, C. Nicollet, B. Soulestin, Textural evolution of polyhedral olivine experiencing rapid cooling rates. *Contrib. Mineral. Petrol.* **153**, 405–416 (2007). doi:10.1007/s00410-006-0154-8
25. M. W. Schmidt, M. Forien, G. Solferino, N. Bagdassarov, Settling and compaction of olivine in basaltic magmas: An experimental study on the time scales of cumulate formation. *Contrib. Mineral. Petrol.* **164**, 959–976 (2012). doi:10.1007/s00410-012-0782-0
26. A. H. Treiman, The nakhlite meteorites: Augite-rich igneous rocks from Mars. *Chem. Erde* **65**, 203–270 (2005). doi:10.1016/j.chemer.2005.01.004
27. F. M. McCubbin, S. M. Elardo, C. K. Shearer Jr., A. Smirnov, E. H. Hauri, D. S. Draper, A petrogenetic model for the comagmatic origin of chassignites and nakhlites: Inferences from chlorine-rich minerals, petrology, and geochemistry. *Meteorit. Planet. Sci.* **48**, 819–853 (2013). doi:10.1111/maps.12095
28. A. Udry, J. M. D. Day, 1.34 billion-year-old magmatism on Mars evaluated from the co-genetic nakhlite and chassignite meteorites. *Geochim. Cosmochim. Acta* **238**, 292–315 (2018). doi:10.1016/j.gca.2018.07.006
29. M. E. Schmidt, C. M. Schrader, T. J. McCoy, The primary fO_2 of basalts examined by the Spirit rover in Gusev Crater, Mars: Evidence for multiple redox states in the martian interior. *Earth Planet. Sci. Lett.* **384**, 198–208 (2013). doi:10.1016/j.epsl.2013.10.005
30. A. H. Treiman, Chemical compositions of martian basalts (shergottites): Some inferences on basalt formation, mantle metasomatism, and differentiation on Mars. *Meteorit. Planet. Sci.* **38**, 1849–1864 (2003). doi:10.1111/j.1945-5100.2003.tb00019.x
31. J. M. D. Day, K. T. Tait, A. Udry, F. Moynier, Y. Liu, C. R. Neal, Martian magmatism from plume metasomatized mantle. *Nat. Commun.* **9**, 4799 (2018). doi:10.1038/s41467-018-07191-0 Medline
32. M. E. Schmidt, T. J. McCoy, The evolution of a heterogeneous Martian mantle: Clues from K, P, Ti, Cr, and Ni variations in Gusev basalts and shergottite meteorites. *Earth Planet. Sci. Lett.* **296**, 67–77 (2010). doi:10.1016/j.epsl.2010.04.046
33. E. M. Stolper *et al.*, The petrochemistry of Jake_M: A martian mugearite. *Science* **341**, 1239463 (2013). doi:10.1126/science.1239463 Medline
34. M. E. Schmidt, J. L. Campbell, R. Gellert, G. M. Perrett, A. H. Treiman, D. L. Blaney, A. Olilla, F. J. Calef III, L. Edgar, B. E. Elliott, J. Grotzinger, J. Hurowitz, P. L. King, M. E. Minitti, V. Sautter, K. Stack, J. A. Berger, J. C. Bridges, B. L. Ehlmann, O. Forni, L. A. Leshin, K. W. Lewis, S. M. McLennan, D. W. Ming, H. Newsom, I. Pradler, S. W. Squyres, E. M. Stolper, L. Thompson, S. VanBommel, R. C. Wiens,

Geochemical diversity in first rocks examined by the Curiosity Rover in Gale Crater: Evidence for and significance of an alkali and volatile-rich igneous source. *J. Geophys. Res. Planets* **119**, 64–81 (2014). doi:10.1002/2013JE004481
35. G. J. Taylor, W. Boynton, J. Brückner, H. Wänke, G. Dreibus, K. Kerry, J. Keller, R. Reedy, L. Evans, R. Starr, S. Squyres, S. Karunatillake, O. Gasnault, S. Maurice, C. d'Uston, P. Englert, J. Dohm, V. Baker, D. Hamara, D. Janes, A. Sprague, K. Kim, D. Drake, Bulk composition and early differentiation of Mars. *J. Geophys. Res.* **112**, E03S10 (2006). doi:10.1029/2005JE002645
36. L. E. Nyquist, D. D. Bogard, C.-Y. Shih, A. Greshake, D. Stöffler, O. Eugster, Ages and geologic histories of Martian meteorites. *Space Sci. Rev.* **96**, 105–164 (2001). doi:10.1023/A:1011993105172
37. M. J. Le Bas, R. W. Le Maitre, A. Streckeisen, B. Zanettin, A chemical classification of volcanic rocks based on the total alkali–silica diagram. *J. Petrol.* **27**, 745–750 (1986). doi:10.1093/petrology/27.3.745
38. A. R. Santos, C. B. Agee, F. M. McCubbin, C. K. Shearer, P. V. Burger, R. Tartèse, M. Anand, Petrology of igneous clasts in Northwest Africa 7034: Implications for the petrologic diversity of the martian crust. *Geochim. Cosmochim. Acta* **157**, 56–85 (2015). doi:10.1016/j.gca.2015.02.023
39. A. C. Allwood, J. A. Hurowitz, Mars 2020 PIXL Raw and Processed Data Bundle. Planetary Data System (2021); doi:10.17189/1522645.
40. L. Beegle, Mars 2020 SHERLOC Bundle. Planetary Data System (2021); doi:10.17189/1522643.
41. J. F. Bell, J. N. Maki, Mars 2020 Mast Camera Zoom Bundle, from Operations Team, calibrated products. Planetary Data System (2021); doi:10.17189/BS6B-4782.
42. T. Barbaer, S. Davidoff, pixlise/piquant: 3.2.11 Open Source. Zenodo (2022); doi:10.5281/zenodo.6959125.
43. T. Barber, pixlise/core: 2.0 open source migration release. Zenodo (2022); doi:10.5281/zenodo.6959096.
44. S. Davidoff, pixlise/pixlise-ui: 2.0 open source migration release. Zenodo (2022); doi:10.5281/zenodo.6959109.
45. T. Barber, pixlise/diffraction-peak-detection: 2.0 open source migration release. Zenodo (2022); doi:10.5281/zenodo.6959138.
46. T. Barber, pixlise/data-formats: 2.0 open source migration release. Zenodo (2022); doi:10.5281/zenodo.6959146.
47. R. C. Moeller, L. Jandura, K. Rosette, M. Robinson, J. Samuels, M. Silverman, K. Brown, E. Duffy, A. Yazzie, E. Jens, I. Brockie, L. White, Y. Goreva, T. Zorn, A. Okon, J. Lin, M. Frost, C. Collins, J. B. Williams, A. Steltzner, F. Chen, J. Biesiadecki, The sampling and caching subsystem (SCS) for the scientific exploration of Jezero Crater by the Mars 2020 Perseverance rover. *Space Sci. Rev.* **217**, 5 (2020). doi:10.1007/s11214-020-00783-7
48. D. A. K. Pedersen, J. Henneke, J. L. Jørgensen, Y. Liu, J. Hurowitz, in *52nd Lunar and Planetary Science Conference*, Abstract #1198 presented at the 52nd Lunar and Planetary Science Conference (2021).
49. C. M. Heirweghet al, Abstract #1260 presented at the 52nd Lunar and Planetary Science Conference (2021).
50. W. Nikonow, D. Rammlmair, Risk and benefit of diffraction in energy dispersive x-ray fluorescence mapping. *Spectrochim. Acta B At. Spectrosc.* **125**, 120–126 (2016). doi:10.1016/j.sab.2016.09.018
51. C. A. Schneider, W. S. Rasband, K. W. Eliceiri, NIH Image to ImageJ: 25 years of image analysis. *Nat. Methods* **9**, 671–675 (2012). doi:10.1038/nmeth.2089 Medline
52. R. R. Loucks, A precise olivine-augite Mg-Fe-exchange geothermometer. *Contrib. Mineral. Petrol.* **125**, 140–150 (1996). doi:10.1007/s004100050211
53. C. K. Shearer, P. V. Burger, J. J. Papike, F. M. McCubbin, A. S. Bell, Crystal chemistry of merrillite from Martian meteorites: Mineralogical recorders of magmatic processes and planetary differentiation. *Meteorit. Planet. Sci.* **50**, 649–673 (2015). doi:10.1111/maps.12355
54. A. Udry, G. H. Howarth, C. D. K. Herd, J. M. D. Day, T. J. Lapen, J. Filiberto, What martian meteorites reveal about the interior and surface of Mars. *J. Geophys. Res. Planets* **125**, 1–34 (2020). doi:10.1029/2020JE006523
55. J. Filiberto, J. Gross, J. Trela, E. Ferré, Gabbroic Shergottite Northwest Africa 6963: An intrusive sample of Mars. *Am. Mineral.* **99**, 601–606 (2014). doi:10.2138/am.2014.4638
56. T. V. Kizovski, K. T. Tait, V. E. Di Cecco, L. F. White, D. E. Moser, Detailed mineralogy and petrology of highly shocked poikilitic shergottite Northwest Africa 6342. *Meteorit. Planet. Sci.* **54**, 768–784 (2019). doi:10.1111/maps.13255
57. G. H. Howarth, J. F. Pernet-Fisher, J. B. Balta, P. H. Barry, R. J. Bodnar, L. A. Taylor, Two-stage polybaric formation of the new enriched, pyroxene-oikocrystic, lherzolitic shergottite, NWA 7397. *Meteorit. Planet. Sci.* **49**, 1812–1830 (2014). doi:10.1111/maps.12357
58. J. Gattacceca, F. M. McCubbin, J. Grossman, A. Bouvier, E. Bullock, H. Chennaoui Aoudjehane, V. Debaille, M. D'Orazio, M. Komatsu, B. Miao, D. L. Schrader, A. J. Timothy Jull, The Meteoritical Bulletin, no. 109. *Meteorit. Planet. Sci.* **56**, 1626–1630 (2021). doi:10.1111/maps.13714
59. R. H. Hewins, M. Humayun, J.-A. Barrat, B. Zanda, J.-P. Lorand, S. Pont, N. Assayag, P. Cartigny, S. Yang, V. Sautter, Northwest Africa 8694, a ferroan chassignite: Bridging the gap between nakhlites and chassignites. *Geochim. Cosmochim. Acta* **282**, 201–226 (2020). doi:10.1016/j.gca.2020.05.021
60. H. Y. McSween*et al.*, Alkaline volcanic rocks from the Columbia Hills, Gusev crater, Mars. *J. Geophys. Res. Planets* **111**, 1–15 (2006).
61. J. Zipfel, C. Schröder, B. L. Jolliff, R. Gellert, K. E. Herkenhoff, R. Rieder, R. Anderson, J. F. Bell III, J. Brückner, J. A. Crisp, Bounce Rock—A shergottite-like basalt encountered at Meridiani Planum, Mars. *Meteorit. Planet. Sci.* **46**, 1–20 (2011). doi:10.1111/j.1945-5100.2010.01127.x
62. A. Cousin, V. Sautter, V. Payré, O. Forni, N. Mangold, O. Gasnault, L. Le Deit, J. Johnson, S. Maurice, M. Salvatore, R. C. Wiens, P. Gasda, W. Rapin, Classification of igneous rocks analyzed by ChemCam at Gale crater, Mars. *Icarus* **288**, 265–283 (2017). doi:10.1016/j.icarus.2017.01.014
63. D. W. Ming, D. W. Mittlefehldt, R. V. Morris, D. C. Golden, R. Gellert, A. Yen, B. C. Clark, S. W. Squyres, W. H. Farrand, S. W. Ruff, R. E. Arvidson, G. Klingelhöfer, H. Y. McSween, D. S. Rodionov, C. Schröder, P. A. de Souza Jr., A. Wang, Geochemical and mineralogical indicators for aqueous processes in the Columbia Hills of Gusev crater, Mars. *J. Geophys. Res.* **111** (E2), n/a (2006). doi:10.1029/2005JE002560
64. R. V. Morris, S. W. Ruff, R. Gellert, D. W. Ming, R. E. Arvidson, B. C. Clark, D. C. Golden, K. Siebach, G. Klingelhöfer, C. Schröder, I. Fleischer, A. S. Yen, S. W. Squyres, Identification of carbonate-rich outcrops on Mars by the Spirit rover. *Science* **329**, 421–424 (2010). doi:10.1126/science.1189667 Medline
65. R. A. Yingst, D. W. Schmidt, M.E., Herkenhoff, K.E. Mittlefehldt, Abstract #3296 presented at the 7th International Conference on Mars (2007).
66. D. W. Mittlefehldt, R. Gellert, T. McCoy, H. Y. McSween, R. Li, Abtract #1505 presented at the 37th Lunar and Planetary Science Conference (2006).
67. M. C. Johnson, M. J. Rutherford, P. Hess, Chassigny petrogenesis: Melt compositions, intensive parameters and water contents of martian magmas. *Geochim. Cosmochim. Acta* **55**, 349–366 (1991). doi:10.1016/0016-7037(91)90423-3
68. Q. He, L. Xiao, W. Hsu, B. Balta, H. Y. McSween, Y. Liu, The water content and parental magma of the second chassignite NWA 2737: Clues from trapped melt inclusions in olivine. *Meteorit. Planet. Sci.* **48**, 474–492 (2013). doi:10.1111/maps.12073
69. L. V. Danyushevsky, F. N. Della-Pasqua, S. Sokolov, Re-equilibration of melt inclusions trapped by magnesian olivine phenocrysts from subduction-related magmas: Petrological implications. *Contrib. Mineral. Petrol.* **138**, 68–83 (2000). doi:10.1007/PL00007664
70. J. Longhi, Complex magmatic processes on Mars—Inferences from the SNC meteorites. *Proc. Lunar Planet. Sci.* **21**, 695–709 (1991).
71. M. E. Minitti, M. J. Rutherford, Genesis of the Mars Pathfinder "sulfur-free" rock from SNC parental liquids. *Geochim. Cosmochim. Acta* **64**, 2535–2547 (2000). doi:10.1016/S0016-7037(00)00366-5
72. J. Filiberto, Experimental constraints on the parental liquid of the chassigny meteorite: A possible link between the chassigny meteorite and a Martian Gusev basalt. *Geochim. Cosmochim. Acta* **72**, 690–701 (2008). doi:10.1016/j.gca.2007.11.007
73. K. R. Stockstill, H. Y. McSween Jr., R. J. Bodnar, Melt inclusions in augite of the Nakhla martian meteorite: Evidence for basaltic parental melt. *Meteorit. Planet. Sci.* **40**, 377–396 (2005). doi:10.1111/j.1945-5100.2005.tb00389.x

74. R. C. F. Lentz, T. J. McCoy, L. E. Collins, C. M. Corrigan, G. K. Benedix, G. J. Taylor, R. P. Harvey, Theo's Flow, Ontario, Canada: A terrestrial analog for the martian nakhlite meteorites, in *Analogs for Planetary Exploration*, vol. 483 (GSA, 2011).
75. D. R. Pyke, A. J. Naldrett, O. R. Eckstrand, Archean ultramafic flows in Munro Township, Ontario. *Geol. Soc. Am. Bull.* **84**, 955–978 (1973). doi:10.1130/0016-7606(1973)84<955:AUFIMT>2.0.CO;2
76. N. T. Arndt, A. J. Naldrett, D. R. Pyke, Komatiitic and iron-rich tholeiitic lavas of Munro Township, Northeast Ontario. *J. Petrol.* **18**, 319–369 (1977). doi:10.1093/petrology/18.2.319
77. W. E. Stone, L. S. Jensen, W. R. Church, Petrography and geochemistry of an unusual Fe-rich basaltic komatiite from Boston Township, Northeastern Ontario. *Can. J. Earth Sci.* **24**, 2537–2550 (1987). doi:10.1139/e87-237
78. W. E. Stone, J. H. Crocket, A. P. Dickin, M. E. Fleet, Origin of Archean ferropicrites: Geochemical constraints from the Boston Creek flow, Abitibi greenstone belt, Ontario, Canada. *Chem. Geol.* **121**, 51–71 (1995). doi:10.1016/0009-2541(94)00126-S
79. M. Murri, M. C. Domeneghetti, A. M. Fioretti, F. Nestola, F. Vetere, D. Perugini, A. Pisello, M. Faccenda, M. Alvaro, Cooling history and emplacement of a pyroxenitic lava as proxy for understanding Martian lava flows. *Sci. Rep.* **9**, 17051 (2019). doi:10.1038/s41598-019-53142-0 Medline
80. J. C. Dann, T. L. Grove, in *Developments in Precambrian Geology*, M. J. van Kranendonk, R. H. Smithies, V. C. Bennett, Eds. (Elsevier, 2007), vol. 15, pp. 527-570.
81. R. T. Helz, Crystallization history of Kilauea Iki lava lake as seen in drill core recovered in 1967-1979. *Bull. Volcanol.* **43**, 675–701 (1980). doi:10.1007/BF02600365
82. H. C. Hardee, Solidification in Kilauea Iki lava lake. *J. Volcanol. Geotherm. Res.* **7**, 211–223 (1980). doi:10.1016/0377-0273(80)90030-X
83. N. Vinet, M. D. Higgins, What can crystal size distributions and olivine compositions tell us about magma solidification processes inside Kilauea Iki lava lake, Hawaii? *J. Volcanol. Geotherm. Res.* **208**, 136–162 (2011). doi:10.1016/j.jvolgeores.2011.09.006
84. I. S. Puchtel, A. W. Hofmann, K. Mezger, A. A. Shchipansky, V. S. Kulikov, V. V. Kulikova, Petrology of a 2.41 Ga remarkably fresh komatiitic basalt lava lake in Lion Hills, central Vetreny Belt, Baltic Shield. *Contrib. Mineral. Petrol.* **124**, 273–290 (1996). doi:10.1007/s004100050191
85. N. T. Arndt, Spinifex and swirling olivines in a komatiite lava lake, Munro Township, Canada. *Precambrian Res.* **34**, 139–155 (1986). doi:10.1016/0301-9268(86)90054-9
86. L. Wilson, J. W. Head III, Mars: Review and analysis of volcanic eruption theory and relationships to observed landforms. *Rev. Geophys.* **32**, 221–263 (1994). doi:10.1029/94RG01113
87. J. D. Macdougall, *Continental Flood Basalts* (Springer, 1988).
88. K. Hon, J. Kauahikaua, R. Denlinger, K. Mackay, Emplacement and inflation of pahoehoe sheet flows: Observations and measurements of active lava flows on Kilauea Volcano, Hawaii. *Geol. Soc. Am. Bull.* **106**, 351–370 (1994). doi:10.1130/0016-7606(1994)106<0351:EAIOPS>2.3.CO;2
89. S. Self, T. Thordarson, L. Keszthelyi, Emplacement of Continental Flood Basalt Lava Flows. *Large Igneous Prov. Cont. Ocean. Planet. Flood Volcanism* (1997), pp. 381–410.
90. S. Self, L. Keszthelyi, T. Thordarson, The Importance of Pahoehoe. *Annu. Rev. Earth Planet. Sci.* **26**, 81–110 (1998). doi:10.1146/annurev.earth.26.1.81
91. N. E. Moore, A. L. Grunder, W. A. Bohrson, The three-stage petrochemical evolution of the Steens Basalt (southeast Oregon, USA) compared to large igneous provinces and layered mafic intrusions. *Geosphere* **14**, 2505–2532 (2018). doi:10.1130/GES01665.1
92. N. Arndt, C. M. Lesher, S. J. Barnes, Komatiite (Cambridge University Press, Cambridge, 2008).
93. J. M. Husch, Palisades sill: Origin of the olivine zone by separate magmatic injection rather than gravity settling. *Geology* **18**, 699–702 (1990). doi:10.1130/0091-7613(1990)018<0699:PSOOTO>2.3.CO;2
94. W. D. Smith, W. Maier, The geotectonic setting, age and mineral deposit inventory of global layered intrusions. *Earth Sci. Rev.* **220**, 103736 (2021). doi:10.1016/j.earscirev.2021.103736
95. O. Namur *et al.*, Igneous layering in basaltic magma chambers, in *Layered Intrusions*, B. Charlier, O. Namur, R. Latypov, C. Tegner, Eds. (2015), pp. 75–152.
96. H. V. Eales, R. G. Cawthorn, The bushveld complex. *Dev. Petrol.* **15**, 181–229 (1996). doi:10.1016/S0167-2894(96)80008-X
97. T. B. Grant, R. B. Larsen, L. Anker-Rasch, K. R. Grannes, M. Iljina, S. McEnroe, E. Nikolaisen, M. Schanche, E. Øen, Anatomy of a deep crustal volcanic conduit system; the Reinfjord ultramafic complex, Seiland Igneous Province, northern Norway. *Lithos* **252–253**, 200–215 (2016). doi:10.1016/j.lithos.2016.02.020
98. J. Filiberto, R. Dasgupta, Fe^{2+}-Mg partitioning between olivine and basaltic melts: Applications to genesis of olivine-phyric shergottites and conditions of melting in the Martian interior. *Earth Planet. Sci. Lett.* **304**, 527–537 (2011). doi:10.1016/j.epsl.2011.02.029
99. Y. Liu, C. Ma, J. R. Beckett, Y. Chen, Y. Guan, Rare-earth-element minerals in martian breccia meteorites NWA 7034 and 7533: Implications for fluid–rock interaction in the martian crust. *Earth Planet. Sci. Lett.* **451**, 251–262 (2016). doi:10.1016/j.epsl.2016.06.041
100. H. Y. McSween Jr., G. J. Taylor, M. B. Wyatt, Elemental composition of the Martian crust. *Science* **324**, 736–739 (2009). doi:10.1126/science.1165871 Medline
101. R. H. Hewins, B. Zanda, M. Humayun, A. Nemchin, J.-P. Lorand, S. Pont, D. Deldicque, J. J. Bellucci, P. Beck, H. Leroux, M. Marinova, L. Remusat, C. Göpel, E. Lewin, M. Grange, A. Kennedy, M. J. Whitehouse, Regolith breccia Northwest Africa 7533: Mineralogy and petrology with implications for early Mars. *Meteorit. Planet. Sci.* **52**, 89–124 (2017). doi:10.1111/maps.12740
102. M. E. Schmidt, M. R. M. Izawa, A. P. Thomas, L. M. Thompson, R. Gellert, Abstract #1571 presented at the 48th Lunar and Planetary Science Conference (2017).
103. J. A. Berger, R. Gellert, N. I. Boyd, P. L. King, M. A. McCraig, C. D. O'Connell-Cooper, M. E. Schmidt, J. G. Spray, L. M. Thompson, S. J. V. VanBommel, A. S. Yen, Elemental composition and chemical evolution of geologic materials in Gale Crater, Mars: APXS results From Bradbury Landing to the Vera Rubin Ridge. *J. Geophys. Res. Planets* **125**, e2020 (2020). doi:10.1029/2020JE006536
104. R. Gellert, R. Rieder, J. Brückner, B. C. Clark, G. Dreibus, G. Klingelhöfer, G. Lugmair, D. W. Ming, H. Wänke, A. Yen, J. Zipfel, S. W. Squyres, Alpha Particle X-Ray Spectrometer (APXS): Results from Gusev crater and calibration report. *J. Geophys. Res.* **111** (E2), n/a (2006). doi:10.1029/2005JE002555
105. D. W. Ming, R. Gellert, R. V. Morris, R. E. Arvidson, J. Brückner, B. C. Clark, B. A. Cohen, C. d'Uston, T. Economou, I. Fleischer, G. Klingelhöfer, T. J. McCoy, D. W. Mittlefehldt, M. E. Schmidt, C. Schröder, S. W. Squyres, E. Tréguier, A. S. Yen, J. Zipfel, Geochemical properties of rocks and soils in Gusev Crater, Mars: Results of the Alpha Particle X-Ray Spectrometer from Cumberland Ridge to Home Plate. *J. Geophys. Res.* **113** (E12), E12S39 (2008). doi:10.1029/2008JE003195
106. D. E. Smith, M. T. Zuber, H. V. Frey, J. B. Garvin, J. W. Head, D. O. Muhleman, G. H. Pettengill, R. J. Phillips, S. C. Solomon, H. J. Zwally, W. B. Banerdt, T. C. Duxbury, M. P. Golombek, F. G. Lemoine, G. A. Neumann, D. D. Rowlands, O. Aharonson, P. G. Ford, A. B. Ivanov, C. L. Johnson, P. J. McGovern, J. B. Abshire, R. S. Afzal, X. Sun, Mars Orbiter Laser Altimeter: Experiment summary after the first year of global mapping of Mars. *J. Geophys. Res.* **106** (E10), 23689–23722 (2001). doi:10.1029/2000JE001364
107. J. L. Dickson, L. A. Kerber, C. I. Fassett, B. L. Ehlmann, paper presented at the 49th Annual Lunar and Planetary Science Conference (2018).
108. J. F. Bell 3rd, J. N. Maki, G. L. Mehall, M. A. Ravine, M. A. Caplinger, Z. J. Bailey, S. Brylow, J. A. Schaffner, K. M. Kinch, M. B. Madsen, A. Winhold, A. G. Hayes, P. Corlies, C. Tate, M. Barrington, E. Cisneros, E. Jensen, K. Paris, K. Crawford, C. Rojas, L. Mehall, J. Joseph, J. B. Proton, N. Cluff, R. G. Deen, B. Betts, E. Cloutis, A. J. Coates, A. Colaprete, K. S. Edgett, B. L. Ehlmann, S. Fagents, J. P. Grotzinger, C. Hardgrove, K. E. Herkenhoff, B. Horgan, R. Jaumann, J. R. Johnson, M. Lemmon, G. Paar, M. Caballo-Perucha, S. Gupta, C. Traxler, F. Preusker, M. S. Rice, M. S. Robinson, N. Schmitz, R. Sullivan, M. J. Wolff, The Mars 2020 *Perseverance* Rover Mast Camera Zoom (Mastcam-Z) Multispectral, Stereoscopic Imaging Investigation. *Space Sci. Rev.* **217**, 24 (2021). doi:10.1007/s11214-020-00755-x Medline
109. R. Bhartia, L. W. Beegle, L. DeFlores, W. Abbey, J. Razzell Hollis, K. Uckert, B. Monacelli, K. S. Edgett, M. R. Kennedy, M. Sylvia, D. Aldrich, M. Anderson, S. A. Asher, Z. Bailey, K. Boyd, A. S. Burton, M. Caffrey, M. J. Calaway, R. Calvet, B. Cameron, M. A. Caplinger, B. L. Carrier, N. Chen, A. Chen, M. J. Clark, S. Clegg, P. G. Conrad, M. Cooper, K. N. Davis, B. Ehlmann, L. Facto, M. D. Fries, D. H. Garrison,

D. Gasway, F. T. Ghaemi, T. G. Graff, K. P. Hand, C. Harris, J. D. Hein, N. Heinz, H. Herzog, E. Hochberg, A. Houck, W. F. Hug, E. H. Jensen, L. C. Kah, J. Kennedy, R. Krylo, J. Lam, M. Lindeman, J. McGlown, J. Michel, E. Miller, Z. Mills, M. E. Minitti, F. Mok, J. Moore, K. H. Nealson, A. Nelson, R. Newell, B. E. Nixon, D. A. Nordman, D. Nuding, S. Orellana, M. Pauken, G. Peterson, R. Pollock, H. Quinn, C. Quinto, M. A. Ravine, R. D. Reid, J. Riendeau, A. J. Ross, J. Sackos, J. A. Schaffner, M. Schwochert, M. O Shelton, R. Simon, C. L. Smith, P. Sobron, K. Steadman, A. Steele, D. Thiessen, V. D. Tran, T. Tsai, M. Tuite, E. Tung, R. Wehbe, R. Weinberg, R. H. Weiner, R. C. Wiens, K. Williford, C. Wollonciej, Y.-H. Wu, R. A. Yingst, J. Zan, Perseverance's scanning habitable environments with raman and luminescence for organics and chemicals (SHERLOC) investigation. *Space Sci. Rev.* **217**, 58 (2021). doi:10.1007/s11214-021-00812-z

ACKNOWLEDGMENTS

We are grateful to Mars 2020 team members who participated in tactical and strategic science operations. Detailed comments by K. Edgett are greatly appreciated. YL thank Laszlo P Keszthelyi for the discussion about Earth and Mars lava flows, Nathan Williams for providing the base maps used in Fig. 1, A and C, and Jim Bell for providing the image used in Fig. 1D. **Funding:** The work described in this paper was partially carried out at the Jet Propulsion Laboratory, California Institute of Technology, under a prime contract with the National Aeronautics and Space Administration (80NM0018D0004). YL, MT, ACA, JAH, CMH, SD, RPH, KAF, KMS, JDT, BC, ELC, KM, LWB, LAW, JPG, AHA, BHNH, JRJ, WTE, SMM, AG, RCW, and KU were supported by NASA grant 80NM0018D0004 through JPL. JRJ was also supported by ASU subcontract 15-707. RCW was also supported by NASA grant NNH13ZDA018O for Supercam to LANL. DTF was supported by Australian Research Council grant DE210100205. EAC was supported by Canadian Space Agency grant 19PACOI0 and Natural Sciences and Engineering Research Council of Canada grant RGPIN-2021-02995. CDKH, TVK, and MES were supported by Canadian Space Agency M2020 Participating Scientist grants. AU, SJV, BAC, MN, DLS, JIS, KLS, TBo and BPW were supported by NASA Mars 2020 Participating Scientist grants. The work of KB, SB, OB, LM, NM, CQN, and VS on Mars 2020 was supported by CNES. KHL was supported by a UK Space Agency Aurora Research Fellowship. TBo was supported by the Simons Foundation Collaboration on the Origins of Life. SG was supported by the UK Space Agency and the Royal Society (grant SRF\R1\21000106). AGF was supported by the European Research Council CoG #818602. **Author contributions:** YL led the writing of the manuscript. YL, MES, AHT, MMT, JAH, ACA, and TK prepared original draft with input from CDKH, AU, NM, SG, KHL, LM, DLS, DCC, FMM, AJB, JIS, SMM, DOF, CQN, BH. All authors provided input to the manuscript through discussion, editing, or reviewing. YL, MMT, MWMJ, DAKP, JAH, TK, SVB, AK, BCC, BJO performed methods and data processing. YL, DAKP, JH prepared visualization with contributions from ACA, MES, MWMJ, MMT, CQN, TK, and AHT. KU and YL made Movie S1. WTE and CMH developed the Piquant software; SD led development of the Pixlise software with PN, AG, and TBa. Project management of PIXL investigation was by ACA as the PIXL principal investigator, JAH as the deputy principal investigator, WTE as the chief spectroscopist, and LAW as the instrument chief engineer. **Competing interests:** The authors declare that they have no competing interests. **Data and materials availability:** All data used in this paper are archived in the NASA Planetary Data System (*39–41*). Image numbers and data sources for the meteorites and other rovers used for comparison are listed in table S7. The source codes for the Pixlise and Piquant software are available at (*42–46*). Our derived elemental abundances are listed in tables S2 to S5.

SUPPLEMENTARY MATERIALS

science.org/doi/10.1126/science.abo2756
Materials and Methods
Supplementary Text
Figs. S1 to S10
Tables S1 to S7
References (*47–109*)
Movie S1

Submitted 24 January 2022; accepted 8 August 2022
Published online 25 August 2022
10.1126/science.abo2756

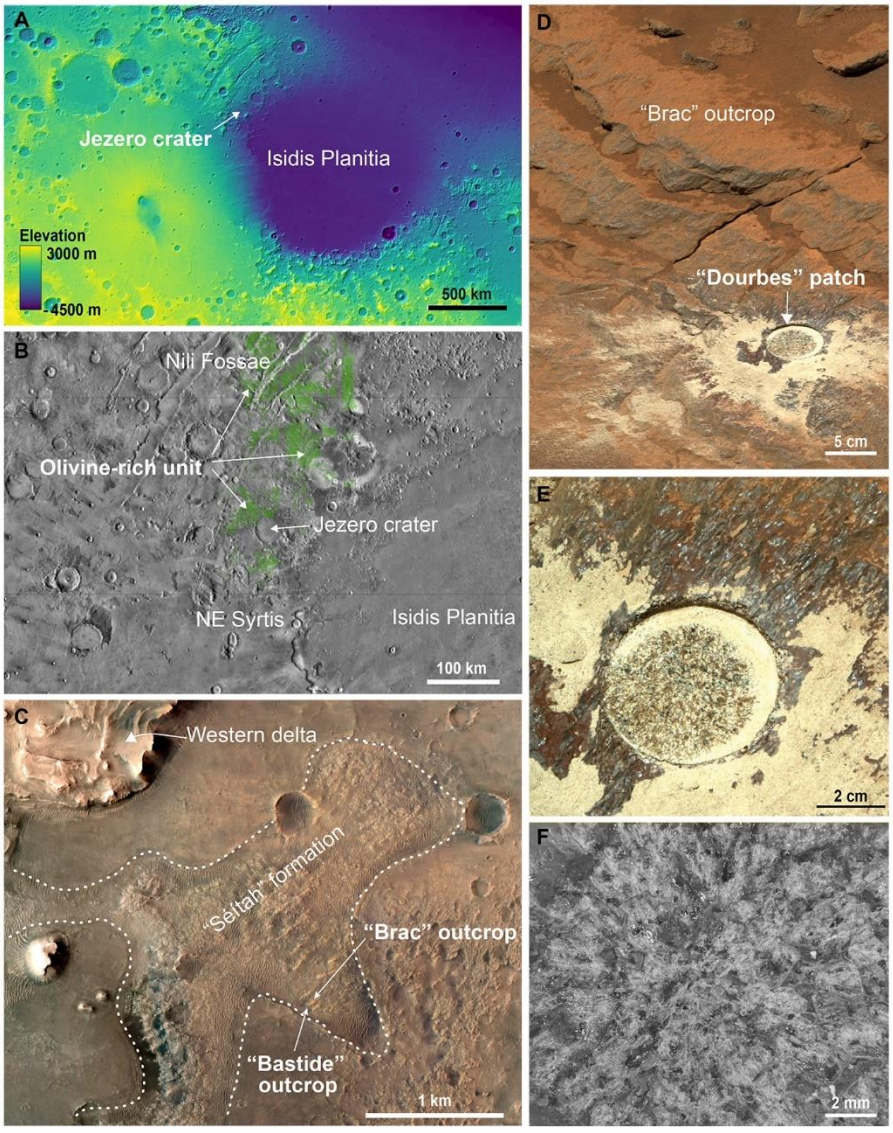

Fig. 1. The Dourbes patch in context from outcrop to regional scale. (**A**) Colorized terrain topography map showing location of Jezero crater on west edge of Isidis Planitia. Color scale bar shows altitude in meters. (**B**) Distribution of the regional olivine-bearing unit (green) on an orbital image. Data from (*2*). (**C**) Color orbital image showing the location of Brac outcrop in the Séítah formation. The dotted white line demarcates the boundary of the Séítah formation outcrops. (**D**) Mast Camera Zoom (Mastcam-Z) image of the Brac outcrop, showing 5-10 cm thick layers and the location of Dourbes patch (5 cm diameter). (**E**) Mastcam-Z image showing more detail of the Dourbes patch. (**F**) A portion of the abraded patch shown by the autofocus and context imager (ACI) of the Scanning Habitable Environments with Raman and Luminescence for Organics and Chemicals (SHERLOC) instrument on Perseverance rover (*5*). Image sources are listed in table S7.

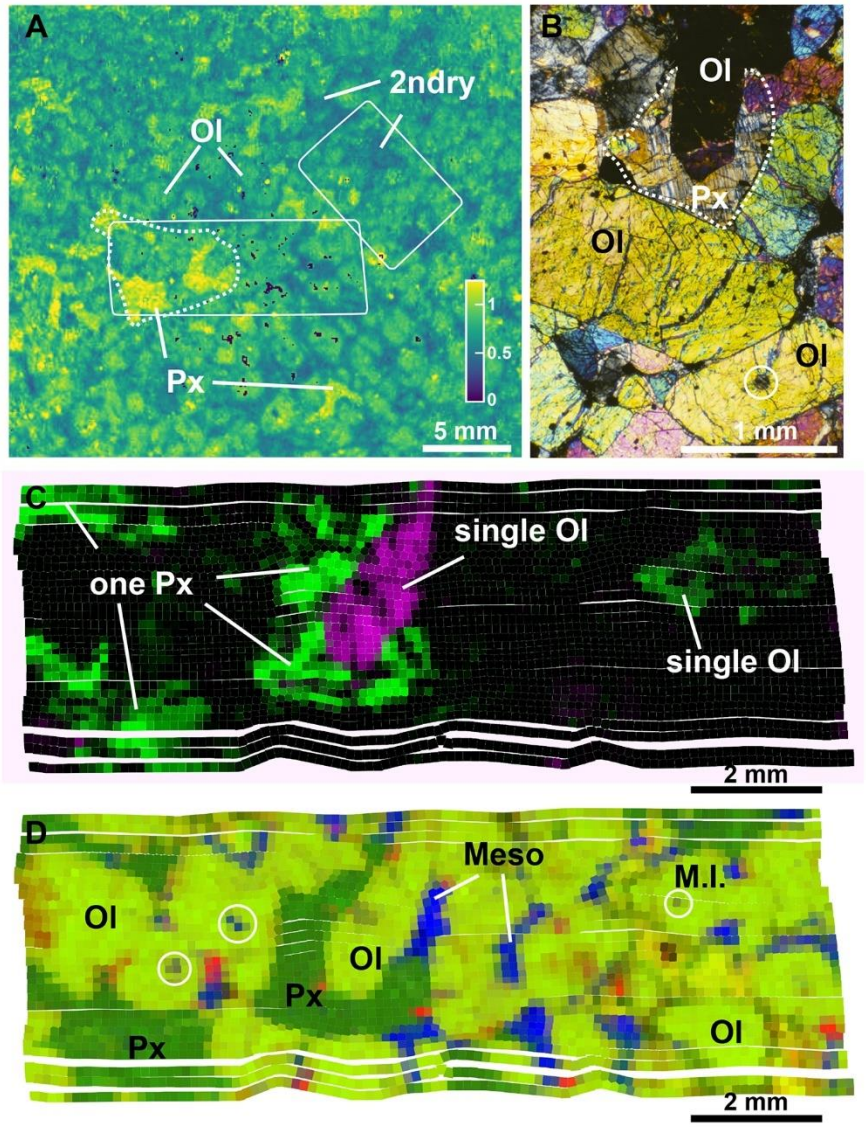

Fig. 2. Cumulate texture of Dourbes. (**A**) Ratio image taken with the PIXL Micro-Context Camera (MCC), showing the G/NIR ratios (color bar). Dourbes has a cumulate texture with olivine grains (labeled Ol) and a poikilitic texture (region within the white dotted line) with pyroxene (labeled Px). Secondary minerals are labeled as 2ndry. White boxes indicate the areas used for x-ray fluorescence scans (figs. S3 and S4), the larger of which shown in panels C and D. (**B**) Cross-polarized light image of the Chassigny meteorite for comparison, showing poikilitic texture. Labels are the same as panel A. The white circle indicates a melt inclusion (M.I.) in Ol. (**C**) Mineral domain clustering map of the same region shown in panel D. Green and magenta are used for two different diffraction peaks (7.28 – 7.72 keV and 5.67 – 6.17 keV, respectively. Points with the same diffraction peak are shown in the same color. All three regions of Px chemistry display the same diffraction peak (all green), suggesting these regions are from a single pyroxene crystal. Ol grains inside the Px grains display different orientations although all points inside one grain display the same diffraction peak (magenta) (*16*). (**D**) Chemical map derived from x-ray fluorescence, showing FeO (red), MgO (green), and Al_2O_3 (blue) concentrations (fig. S3 shows grayscale images of each element). Labels indicate olivine, pyroxenes, and mesostasis (Meso). Blue circles indicate M.I.s. These composition maps are shown in context with other optical images in movie S1.

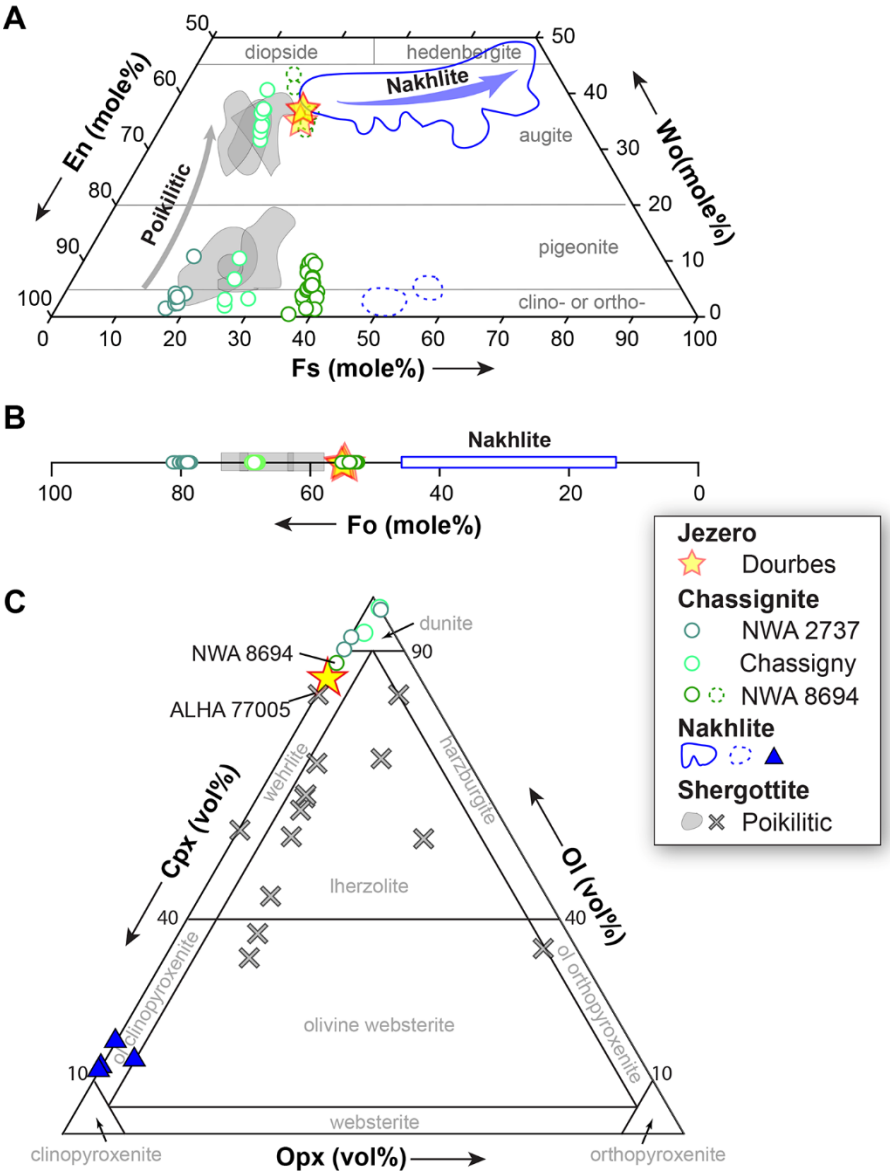

Fig. 3. Mineralogy of Dourbes. (A) Classification of pyroxene using the percentage compositions of wollastonite (Wo), enstatite (En), and ferrosilite (Fs) (*17*). The average compositions of Dourbes pyroxene grains in table S3 are shown as star symbols. Symbols or fields with solid lines show volumetrically major pyroxene species and those with dotted blue lines are minor pyroxene species. Arrows show the direction of crystallization. (B) Binary diagram showing mole percentage of forsterite (Fo) in the olivine (Ol). The average compositions of Dourbes olivines (table S2) are shown as star symbols. Dourbes olivine and pyroxene differ from Martian meteorites. (C) Classification of ultramafic rocks using volume percentages of olivine (Ol), clinopyroxene (Cpx) and orthopyroxene (Opx) (*18*). Symbols are indicated in the legend. Source data for meteorites are listed in table S7.

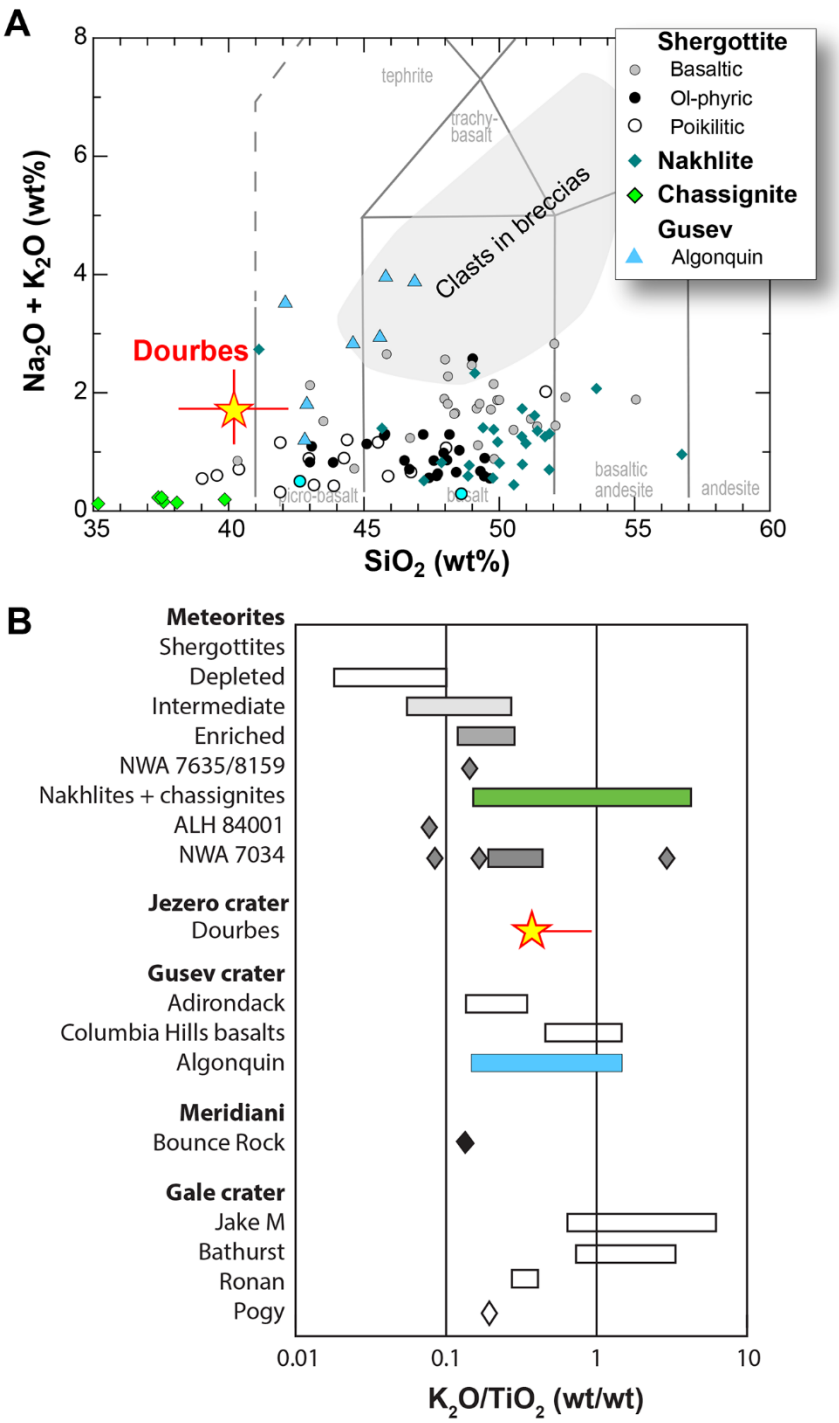

Fig. 4. Bulk chemistry of Dourbes compared to meteorites and igneous rocks elsewhere on Mars. (**A**) Plot of total alkali oxides as a function of SiO_2 abundance. Fields defined by vertical gray lines show the classification of volcanic rocks (*37*). The gray field shows igneous clasts in breccia meteorite NWA 7034 (*38*). Dourbes contains less SiO_2 and higher alkali metal oxides than other Martian igneous rocks. (**B**) Weight percentage ratios of K_2O/TiO_2 for Dourbes and other Martian igneous rocks. Horizontal bars show the range of values from different samples of the listed targets. Filled diamonds show individual samples. Dourbes is most similar to K-enriched meteorites, such as chassignite and nakhlite, and the Algonquin rock in Gusev crater. Dourbes data are plotted as star symbols with the error bar indicating the estimated 1σ uncertainty. Dourbes data are listed in table S5 and data sources for meteorites and rover data are listed in table S7.

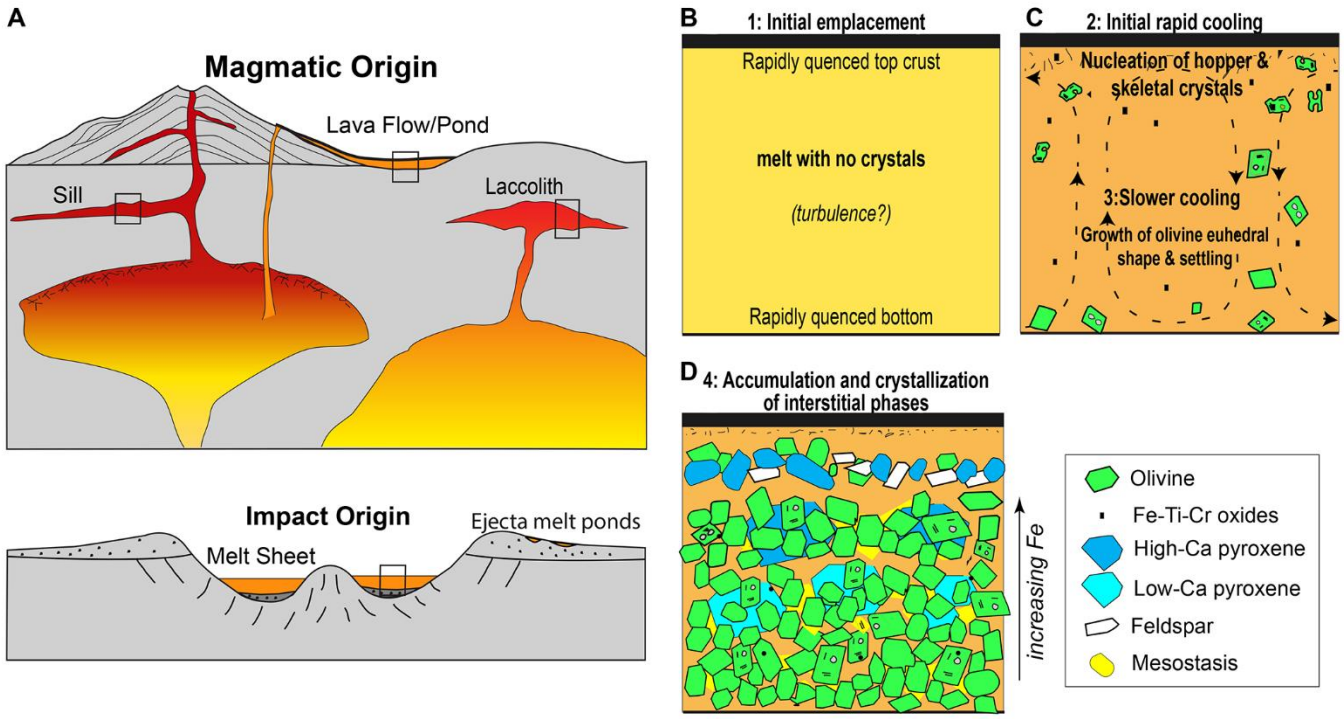

Fig. 5. Schematic diagram of potential emplacement models. (A) Potential emplacement models for the Bastide member, which hosts the Brac and Batide outcrops. Color hue schematically indicates the temperature of the melt, with darker being cooler. Possible scenarios are an extrusive lava flow/pond, an intrusive sill or a small laccolith, or an impact melt sheet or ejecta melt pond. All models provide the range of cooling rates as we infer for the Brac outcrop. Panels B-D show the petrology of our model (not to scale). (B) Initial emplacement of melt without any crystals, forming a rapidly quenched top crust and bottom. (C) Rapid cooling after emplacement causes nucleation and growth of hopper or skeletal olivine grains near the top surface. Convection of olivine into the (more slowly cooling) interior promotes olivine growth. Once each crystal reaches a critical size, it sinks to the bottom. (D) Continued cooling, crystallization and sinking concentrates olivine at the base. Further crystallization of low-Ca pyroxene, high-Ca pyroxene and other minerals (indicated in the legend) form stratified layers, with increasing Fe contents higher in the melt body.

An olivine cumulate outcrop on the floor of Jezero crater, Mars

Y. LiuM. M. TiceM. E. SchmidtA. H. TreimanT. V. KizovskiJ. A. HurowitzA. C. AllwoodJ. HennekeD. A. K. PedersenS. J. VanBommelM. W. M. JonesA. L. KnightB. J. OrensteinB. C. ClarkW. T. ElamC. M. HeirweghT. BarberL. W. BeegleK. BenzeraraS. BernardO. BeyssacT. BosakA. J. BrownE. L. CardarelliD. C. CatlingJ. R. ChristianE. A. CloutisB. A. CohenS. DavidoffA. G. FairénK. A. FarleyD. T. FlanneryA. GalvinJ. P. GrotzingerS. GuptaJ. HallC. D. K. HerdK. Hickman-LewisR. P. HodyssB. H. N. HorganJ. R. JohnsonJ. L. JørgensenL. C. KahJ. N. MakiL. MandonN. MangoldF. M. McCubbinS. M. McLennanK. MooreM. NachonP. NemereL. D. NothdurftJ. I. NúñezL. O'NeilC. M. Quantin-NatafV. SautterD. L ShusterK. L. SiebachJ. I. SimonK. P. SinclairK. M. StackA. SteeleJ. D. TarnasN. J. ToscaK. UckertA. UdryL. A. WadeB. P. WeissR. C. WiensK. H. WillifordM.-P. Zorzano

Science, **Ahead of Print** • DOI: 10.1126/science.abo2756